Nanoscale

Accepted Manuscript

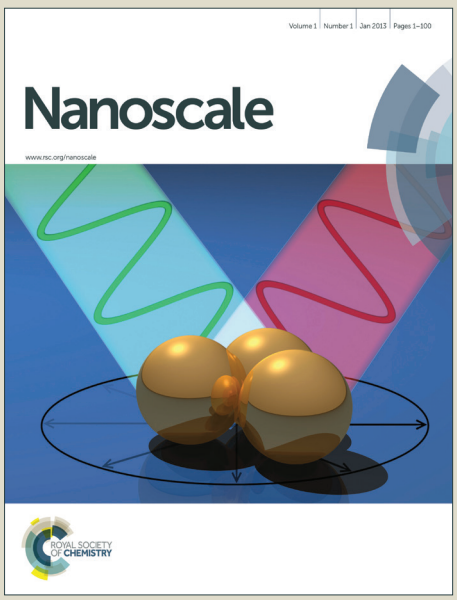

ROYAL SOCIETY OF CHEMISTRY

www.rsc.org/nanoscale

Cite this: DOI: 10.1039/c0xx00000x

www.rsc.org/xxxxxx

ARTICLE TYPE

Efficient Planar Heterojunction Perovskite Solar Cell Employing Graphene Oxide as Hole Conductor

Zhongwei Wu,[a] Sai Bai,[b] Jian Xiang,[a] Zhongcheng Yuan,[a] Yingguo Yang,[c] Wei Cui,[a] Xingyu Gao,[c] Zhuang Liu,[a] Yizheng Jin,[b] and Baoquan Sun*[a]

Received (in XXX, XXX) Xth XXXXXXXXX 20XX, Accepted Xth XXXXXXXXX 20XX
DOI: 10.1039/b000000x

Graphene oxide (GO) is employed as a hole conductor in inverted planar heterojunction perovskite solar cells, and the devices with $CH_3NH_3PbI_{3-x}Cl_x$ as absorber achieve an efficiency of over 12%. The perovskite film grown on GO exhibits enhanced crystallization, high surface coverage ratio as well as preferred in-plane orientation of (110) plane. Efficient hole extraction form the perovskite to GO is demonstrated.

Introduction

Solution-processable solar cells are attractive owing to their cost- and energy-efficient merits for large-scale and flexible application compared with established crystalline silicon photovoltaics.[1] Organic solar cell (OPV) and dye sensitized solar cell (DSSC) as two significant representatives have been taken tremendous efforts to boost their power conversion efficiency (PCE). Nowadays, both of them can achieve over 10% efficiencies by comprehensive material design, structure optimization and molecule engineering.[2-5] However, perovskite-based solar cell with encouraging efficiency of over 15% becomes an important player in the field of photovoltaics,[6, 7] which has been considered as a feasible candidate that can address the low-cost solution process and outstanding efficiency simultaneously.[8, 9]

Organometal halide perovskite, possessing a direct band gap, large absorption and high carrier mobility, was first used in the DSSC as sensitizer and the device achieved an efficiency of 3.81%.[10] However this type of device exhibited poor stability due to the sensitizer dissolved by the liquid electrolyte. Subsequently, replacing the electrolyte with a solid organic conductor rendered improved device performance and stability,[11-14] and even boosted the efficiency over 10%. Since then, 12%-15% efficiencies were frequently achieved by material and structure optimization.[15-18] Behind the high performance of the device, the long electron-hole diffusion lengths exceeding 1 μm and 100 nm in $CH_3NH_3PbI_2Cl$ and $CH_3NH_3PbI_3$ films respectively were uncovered,[19, 20] which were extremely larger than the exciton diffusion length in conjugated polymer. Such long electron-hole diffusion length justifies the high-performance planar heterojunction (PHJ) perovskite solar cell.

Two architectures are symbiotic in the perovskite-based solar cell: meso-superstructured solar cells and PHJ perovskite solar cells. Meso-superstructured device consists of a metal-oxide (such as TiO_2, Al_2O_3) scaffold infiltrated with the pervoskite. Although the meso-superstuctured device has the champion efficiency, homogeneous infiltration of the perovskite precursor remains an issue, which results in a large standard deviations existing in the meso-superstuctured device.[11, 15] PHJ structure, a perovskite absorber sandwiched between electron and hole conductors, avoids the pore filling problem and simplifies the device fabrication process without sacrificing the efficiency compared to the meso-superstructured device.[18, 21, 22] In the PHJ structure, the conductor (also called n- or p-type quencher) plays a critical role in the device working mechanism. An efficient conductor assures the charge transfer at cathode or anode interface, thereby guiding the charge transport to corresponding electrode selectively. Although some conductor-free (hole or electron conductor) devices were demonstrated, their PCEs remained mediocre.[23, 24] Known from the originally emerged PHJ perovskite solar cell with a structure of fluorine-doped tin oxide (FTO)/TiO_2/perovskite/2-7,7'-tetrakis(N,N-di-p-methoxyphenylamine)-9,9-spirobifluorene (Spiro-OMeTAD/Ag),[21] phenyl-C61-butyric acid methyl ester (PCBM) and poly(3,4-ethylenedioxythiophene)poly(styrenesulfonate) (PEDOT:PSS) are the most efficient n- and p-type conductor in the so-called inverted PHJ perovskite solar cell respectively, where holes are collected through the transparent conductive oxide (TCO) anode and electrons through the metal cathode. The inverted structure is suitable to fabricate low-temperature (below 150 ℃) solution-processable perovskite device and compatible with flexible substrate.[25-27] The inverted devices based on PCBM and PEDOT:PSS as conductors have achieved efficiencies of 10-11%.[28, 29] Recently, NiO_x has been demonstrated another efficient hole conductor in the $CH_3NH_3PbI_3$-based inverted planar cell with a efficiency of 7.8%.[30] However, outstanding and stable conductors are still rarely developed and applied in the inverted PHJ perovskite device. Therefore implementation of innovative interfacial materials is still essential to maximize the device performance.

Recently, nanocomposites of graphene and TiO_2 nanoparticles was utilized as the electron collection layers in meso-superstructured perovskite solar cells, extremely decreasing the processing temperature from 500 ℃ to 150 ℃.[31] Furthermore, an ultrathin graphene quantum dots (GQDs) layer between perovskite and TiO_2 significantly enhanced perovskite solar cells

performance. It was found that the inserted GQDs dramatically enhanced the electron extraction.[32] These successful attempts indicate that the graphene-based derivatives have the potential to contribute significantly toward high-performance perovskite solar cell.

Herein, an intimate graphene derivative, grapheme oxide (GO), is first introduced into the perovskite solar cell as a hole conductor. An inverted PHJ perovskite solar cell, employing $CH_3NH_3PbI_{3-x}Cl_x$ as absorber and GO as hole conductor, achieves a champion PCE of 12.4%. The charge transfer between GO and the perovskite, morphology and crystallization of the perovskite film grown on GO are also investigated.

Experimental section

Materials and sample preparation

Methylammonium iodide (MAI) was synthesized according to the literature.[11] Colloidal ZnO nanocrystals were synthesized by a solution-precipitation process according to literature procedures.[33] GO was obtained from a modified Hummer's method with flake expandable graphite used as the original material according to a previous protocol.[34, 35] PCBM and PEDOT:PSS (CLEVIOS Al 4083) were purchased from Solenne and Heraeus.

To prepare the perovskite precursor solution, MAI and lead chloride ($PbCl_2$, 99.999%, Alfa) powder were mixed in anhydrous dimethylformamide (DMF, amine free; 99.9%, Aldrich) with a molar ratio of 3:1. The perovskite precursor solution was stirred at 60 ℃ overnight and filtered through PTFE filters (0.45 μm) before use.

Fabrication of inverted planar perovskite solar cells

The glass substrate coated with patterned indium tin oxide (ITO) with a sheet resistance of ~10 Ω sq^{-1} was cleaned with detergent, ultrasonicated in acetone and ethanol, and then blow dried by nitrogen. Subsequently, the substrates were treated by ultraviolet ozone plasma for 15 min. PEDOT:PSS and GO aqueous solution were spin-coated onto the substrates at 5000 r.p.m. for 60 s. After baked at 120 ℃ for 20 min，the substrates were transferred into a glovebox for absorbing layer coating and electrode deposition. A 40 wt.% $CH_3NH_3PbI_{3-x}Cl_x$ precursor solution was spin-coated at 6000 r.p.m. for 40 s. After laid at the petri dish at room temperature for ~15 min, the perovskite films were annealed on a hot plate at 100 ℃ for ~ 20 min, allowing the color of the films to convert into dark brown. The PCBM layers were deposited from a 30 mg/mL chlorobenzene solution at 2000 r.p.m. Subsequently, the ZnO layers were formed by spin-coating a colloidal ZnO nanocrystal solution (8 mg/mL in ethanol) at 3000 r.p.m. for 40 s. Finally, 150-nm-thick Al was evaporated through a shadow mask under 10^{-6} Torr (Mini spectra, Kurt J. Lesker). The area of each device was 7.25 mm^2 determined by a shadow mask.

Characterization

Device characteristics, current density-voltage (J–V) curves, were measured in a glovebox under a Newport 94023A solar simulator equipped with a 300 W Xenon lamp and an air mass (AM) 1.5G filter was used to generate simulated AM 1.5G solar spectrum irradiation source. The irradiation intensity was 100 mW/cm^2 calibrated by a Newport standard silicon solar cell 91150. A Newport monochromator 74125 and power meter 1918 with silicon detector 918D were used in the external quantum efficiency (EQE) measurements. All electrical data were recorded by a Keithley 2612. The steady-state photoluminescence (PL) measurements were acquired using an Edinburgh Instruments FLS920 fluorescence spectrometer. The atomic force microscopy (AFM) topography image was taken using a MultiMode V (Veeco) operated in the tapping mode. Scanning electron microscopy (SEM) images were obtained from a field emission scanning electron microscope (FEI Quanta 200). Optical characterization was conducted on a UV-Vis spectrophotometer (PerkinElmer Lambda 750). The thickness of GO was determined by ellipsometer and the thick GO layer was confirmed by cross-sectional SEM measurement. The grazing incidence X-ray diffraction (GIXRD) measurements were performed at the BL14B1 beamline of the Shanghai Synchrotron Radiation Facility (SSRF). Two-dimensional (2D) GIXRD patterns were acquired by a MarCCD mounted vertically at a distance ~223 mm from the sample, the grazing incidence angle of X-ray was 0.2 ° and exposure times < 20 sec. The 2D GIXRD patterns were analyzed using the FIT2D software and displayed in scattering vector q coordinates, where $q = 4\pi\sin\theta/\lambda$, θ is half of the diffraction angle, and λ is the X-ray wavelength. Conventional XRD measurement was conducted using a PANalytical (Empyrean) equipment. In the characterizations, the needed layers in samples were prepared just following the device fabrication procedure. For optical and XRD measurements, the perovskite films were sealed by spin-coating a layer of poly(methylmethacrylate) (PMMA) on top.

Results and discussion

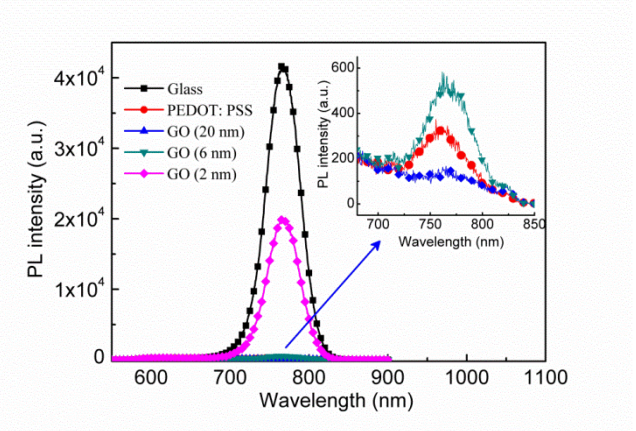

Fig. 1 Steady-state PL spectra for $CH_3NH_3PbI_{3-x}Cl_x$ coated on the different substrates

GO was applied as hole transporting layer in polymer solar cells owing to its suitable work function (~4.9 eV) and acceptable vertical resistivity or its surface doping effect on the active layer,[36-38] which assured the matched energy alignment and unrestricted hole transport at the electrode-active layer interface. In order to utilize the GO as an efficient hole conductor in PHJ perovskite solar cell, charge transfer between the perovskite and GO was monitored by a PL measurement. The perovskite films were deposited on GO films with thickness of ~2, ~6 and ~20 nm,

respectively. These GO films were obtained by spin-coating from its neutral aqueous suspensions with concentrations of 0.25 mg/ml (~2 nm), 1 mg/ml (~6 nm) and 4 mg/ml (~20 nm), respectively. As showed in **Fig. 1**, the PL intensity is quenched when $CH_3NH_3PbI_{3-x}Cl_x$ is coupled with GO, indicting the charge transfer happens between them. In addition, the thicker GO is, the more seriously PL quenching happens.

Table 1. Steady-state PL quenching efficiencies for $CH_3NH_3PbI_{3-x}Cl_x$ coated on different hole conductors

Hole conductor	W/O	GO (0.25 mg/ml)	GO (1 mg/ml)	GO (4 mg/ml)	PEDOT:PSS
Quenching efficiency	/	52.8%	97.9%	98.9%	98.5%

As listed in **Table 1**, the PL quenching efficiency is roughly evaluated by integrating the PL spectra over wavelength and comparing with the pristine perovskite layer. 2-nm-thick GO displays a quenching efficiency of 52.8%, which is comparable with the value of TiO_2 (47%).[39] When the GO thickness is increased to 20 nm, PL is almost completely quenched with an efficiency of 98.9%, which is slightly higher than the quenching efficiency of PEDOT:PSS. Up to now, most high-performing regular perovskite cell is fabricated using TiO_2 as an electron conductor.[7] In another word, 2-nm-thick GO is sufficient to afford a high-performance device if only considering the charge transfer process. The different quenching efficiencies of ~2 nm, ~6 nm and ~20 nm GO may be correlated with the GO coverage on ITO as well as its roughness. Larger coverage ratio and higher roughness will lead to enhanced contact area between perovskite and GO, and then render more efficient charge transfer. Generally, a thick GO film will result in a larger coverage ratio and higher roughness, which has been investigated by previous report.[36] As showed in **Fig. S1**, the GO used here exhibits few-layered sheets with a typical thickness of ~2 nm. Indeed, the SEM images of GO on ITO indicate that the thicker GO, spin-coated from high suspension concentration, achieves a better coverage on ITO (**Fig. S2**).

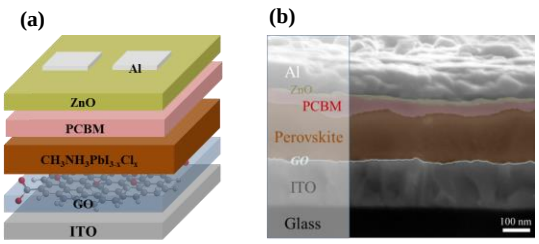

Fig. 2 (a) Schematic of the inverted photovoltaic device configuration consisting of a structure of ITO/GO/$CH_3NH_3PbI_{3-x}Cl_x$/PCBM/ZnO/Al. (b) Cross-sectional SEM image of the optimized inverted device configuration.

Motived by the outstanding charge transfer between GO and perovskite, we fabricated inverted PHJ perovskite solar cell with the structure of ITO/GO/$CH_3NH_3PbI_{3-x}Cl_x$ (170 nm)/PCBM (60 nm)/ZnO (20 nm)/Al (**Fig. 2**a). As illustrated in **Fig. 2**b, the cross-sectional SEM image of device shows distinguishable planar layer-by-layer structure. A thick GO-based device has identified and visible GO layer in the cross-sectional SEM image, which is showed in **Fig. S3**. By tuning the concentrations of GO neutral aqueous suspensions from 0.25 mg/ml to 4 mg/ml, GO with thickness of ~2 nm to ~20 nm can be obtained. In addition, the as-prepared GO film exhibits good solvent resistance (**Fig. S4**), which assures the robust and unique interfacial role of GO in the devices.

Table 2. The photovoltaic parameters of inverted PHJ perovskite solar cells with different hole conductors

Hole conductor layers	Concentration (mg/ml)	V_{oc} [a] (V)	J_{sc} [a] (mA/cm^2)	FF [a]	PCE [a] (%)	R_s (Ω cm^2)
GO	4	0.84	12.88	0.73	7.90	5.81
	2	0.92	13.71	0.72	9.08	5.65
	1	0.99	14.50	0.64	9.19	5.26
	0.5	0.99	15.02	0.67	9.96	5.08
	0.25	0.99	15.59	0.72	11.11	4.98
PEDOT:PSS	/	0.93	15.09	0.66	9.26	6.94
W/O	/	0.55	11.70	0.41	2.64	13.89

[a] All the photovoltaic parameters are the average of a batch of six devices

Table 2 summarizes the photovoltaic parameters of devices measured under AM 1.5G solar illumination at 100 mW/cm^2. As presented from the data, the presence of an efficient hole conductor is critical to achieve a high-performance device. The common PEDOT:PSS-based device results in an efficiency of 9.26%, extremely improved from the original 2.64% efficiency for the device without hole conductor. Regarding to the devices employing GO as hole conductor, over 7% efficiencies can be obtained. When an ultra-thin GO (~2 nm) is employed by depositing from the 0.25 mg/ml GO solution, a PCE over 11% is obtained, corresponding to an open circuit voltage (V_{oc}) of 0.99 V, a short circuit current density (J_{sc}) of 15.59 mA/cm^2, a fill factor (FF) of 0.72. Increasing the GO thickness decreases the transmittance of anode (**Fig. S5**) and increases the series resistance (R_s), which leads to lower J_{sc}. In addition, it is unclear that over thick GO film also results in a reduced V_{oc}. Another parameter, FF, exceeds 70% in either thick or ultra-thin GO-based device, and shows an inferior value in the moderately thick one. We assume that it is determined by the balance between electron and hole transporting to the corresponding electrodes as well as the R_s in device. Generally, in order to cover the rough perovskite surface, the n-type quencher, PCBM, has to be thick enough to achieve a high surface coverage ratio.[28] The PCBM layer used here is ~60 nm. Plus the 20 nm ZnO, electron need to travel a ~80-nm-distance from perovskite-PCBM interface to Al

cathode. The length for hole transporting from perovskite-GO interface to ITO anode is from 2 nm to 20 nm. However, long-range balanced electron- and hole-transport length and mobilities in perovskite are proved,[20, 40] which means the balanced electron- and hole-transport in our planar device is only determined by the electron and hole conductors. For thick GO (20 nm) case, the charge generation rate for electron (PCBM: PL quenching efficiency: 91%) and hole (GO: PL quenching efficiency: 98.9%) is comparable. A relatively thick GO film balances the electron and hole transporting, decreases the charge recombination and results in a high FF. For devices based on ultra-thin GO (2 nm), the smallest R_s leads to a high FF. Interestingly, as indicated in **Fig. S6**, our GO-based device tested in nitrogen didn't show the recently reported PCE variation phenomenon under different sweep direction in the J-V measurement.[41]

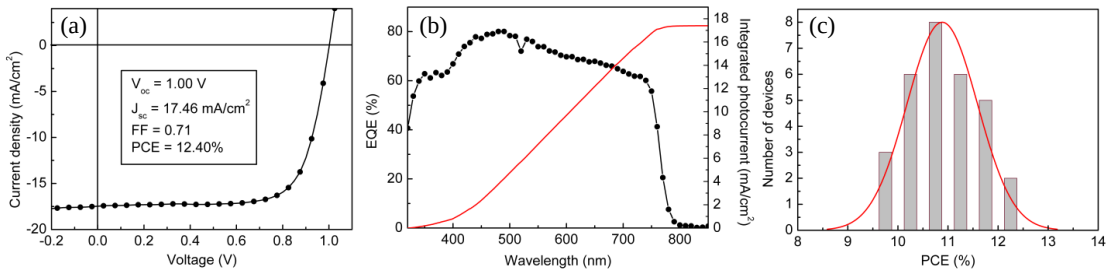

Fig. 3 (a) J–V curve and (b) EQE spectrum of the champion device employing 2 nm GO as hole conductor. (c) Histogram of PCEs measured from 30 devices

Fig. 3 shows the J-V characteristic, EQE spectrum of a champion device and the histogram of efficiencies of devices with 2 nm GO as hole conductor. The champion device exhibits a V_{oc} of 1.00 V, a J_{sc} of 17.46 mA/cm^2, a FF of 0.71, yielding a PCE of 12.40%. The J_{sc} calculated by integrating the EQE curve with an AM 1.5G reference spectrum is 17.39 mA/cm^2, which is very consistent with the corresponding J_{sc} obtained from the J-V curves. Histogram of efficiencies measured from a batch of 30 devices shows an average PCE of 10.88% and a relative standard deviation of 7.06% in PCE. These encouraging results demonstrate GO is an efficient hole conductor to obtain high-performance perovskite solar cell again.

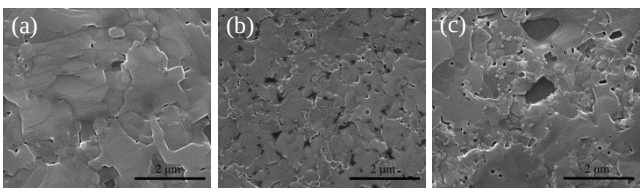

Fig. 4 SEM images of perovskite films ($CH_3NH_3PbI_{3-x}Cl_x$) on the different substrates: (a) ITO/GO; (b) ITO/PEDOT:PSS and (c) bare ITO.

Morphology of the perovskite film, possessing a uniform coverage, plays a key role on the device performance. As shown in the SEM images of the perovskite films on the different substrates (**Fig. 4**), GO and PEDOT:PSS obviously improve the formation and growth of perovskite film, leading to homogeneous surface coverage compared with the bare ITO. Additionally, the insertion of GO allows the perovskite film to grow into larger textured domains, resulting in a nearly full coverage (**Fig. S7**). On the contrary, there are many pores in the film grown on PEDOT:PSS, indicating that the existence of GO film enhances the coverage ratio of perovskite film. GO-based device exhibits lowered dark current (**Fig. S8**), which is consistent with the improved film coverage. As indicated in **Fig. S9**, the perovskite film on GO shows more rough characteristics on the large scale compared with the film on PEDOT:PSS, which will enhance its light harvest capability due to the enhanced light scattering. The combined effects of better coverage, larger domains and rougher surface enhance the absorption of perovskite film in the range from 450 nm to 790 nm (**Fig. S10**) The abrupt absorption peak at ~400 nm for the film on PEDOT:PSS is contributed from the anti-reflection effect of PEDOT:PSS film on ITO, which is consistent with transmittance of the PEDOT:PSS-coated ITO substrate. Generally speaking, the GO attached on the ITO substrate offers a positive effect on the growth of perovskite film, resulting in a uniform and overlapped coverage with large textured domains.

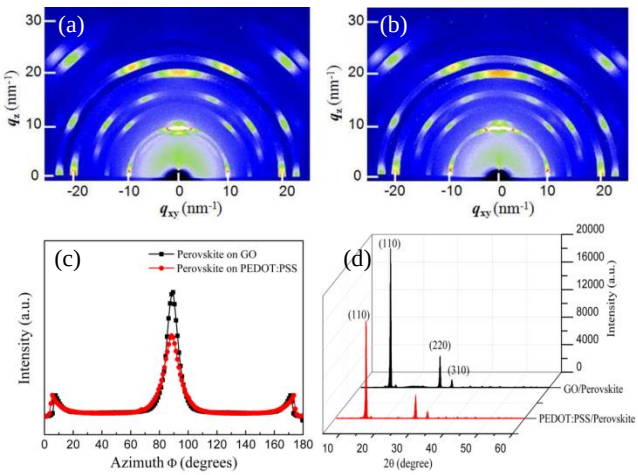

Fig. 5 2D GIXRD profiles of perovskite films on (a) ITO/GO (~2 nm) and (b) ITO/PEDOT:PSS substrates.(c) Radially integrated intensity plots along the ring at q=10 nm^{-1}, assigned to the (110) plane of $CH_3NH_3PbI_{3-x}Cl_x$ perovskite structure. (d) Conventional XRD spectra of perovskite films on quartz /GO (2 nm) and quartz /PEDOT:PSS substrates

Very recently, it was found that processing condition could affect the crystallization and crystal plane orientation of the perovskite film.[42, 43] It was found that a short rapid thermal annealing resulted in the growth of large micron-sized textured perovskite domains with more preferential in-plane orientation of (110) plane. The corresponding device based on large perovskite domain size displayed enhanced performance.[42] Also improved crystallization and in-plane orientation of (110) plane can be

achieved by additive procedure.[29] Apart from the large perovskite domains formed on GO, which is proved by the SEM images, more information should be collected to evaluate the quality of perovskite film. As shown in conventional XRD spectra (**Fig. 5**d), the $CH_3NH_3PbI_{3-x}Cl_x$ perovskite films grown on PEDOT:PSS and GO substrates exhibit a set of strong peaks at 14.1°, 28.5° and 31.9°, corresponding to (110), (220), and (310) crystal planes of a mixed-halide perovskite with an orthorombic crystal structure.[7, 11, 28, 29] The strong and sharp (110) peaks imply the films possess good crystallization and large crystal size. Furthermore, GIXRD measurement was conducted to investigate the crystal plane orientation further. **Fig. 5**a, b shows 2D GIXRD profiles of perovskite films on GO and PEDOT:PSS. Extremely similar diffraction profiles in both samples with spotty patterns were obtained, indicating highly textured perovskite crystal domains formed on both GO and PEDOT:PSS layer. The perovskite domains with high-quality crystallization may be one of the reasons that the PCEs of GO- and PEDOT:PSS-based planar devices can be easily pushed to around 10%. In addition, as indicated in **Fig. 5**c, radially integrating intensity plots along the ring at q=10 nm^{-1} is assigned to the (110) plane of $CH_3NH_3PbI_{3-x}Cl_x$ perovskite structure. Both samples suggest a preferential in-plane orientation with sharp peaks at the azimuth angle of 90°. The perovskite grown on GO seems to give higher orientation order than that on PEDOT:PSS, as indicated by the relatively sharper peaks.

Conclusions

In summary, we have successfully developed GO as hole conductor for the PHJ perovskite solar cell, and a champion efficiency up to 12.4% has been demonstrated. The underlaid GO layer can extract the hole out of the perovskite efficiently, facilitate the formation of homogenous large domains and improve the surface coverage. In addition, the perovskite film grown on GO possess highly textured perovskite crystal domains and preferential in-plane orientation of (110) palne indicated by GIXRD measurement. All these comprehensive information (e.g. domain size, coverage, crystal orientation) maybe provide guideline to develop morphology- and crystallization-compatible interlayer towards high-performance PHJ perovskite solar cell.

Acknowledgement

This work was supported by the National Basic Research Program of China (973 Program) (2012CB932402), the National Natural Science Foundation of China (61176057, 91123005, 61211130358), the Priority Academic Program Development of Jiangsu Higher Education Institutions.

Notes and references

[a] *Jiangsu Key Laboratory for Carbon-Based Functional Materials & Devices, Institute of Functional Nano & Soft Materials (FUNSOM) and Collaborative Innovation Center of Suzhou Nano Science and Technology, Soochow University, 199 Ren'ai Road, Suzhou, 215123, People's Republic of China; E-mail: bqsun@suda.edu.cn*

[b] *State Key Laboratory of Silicon Materials, Cyrus Tang Center for Sensor Materials and Applications, Department of Materials Science and Engineering, Zhejiang University, Hangzhou 310027, People's Republic of China*

[c] *Shanghai Synchrotron Radiation Facility, Shanghai Institute of Applied Physics, Chinese Academy of Sciences, 239 Zhangheng Road, Pudong New Area, Shanghai 201204, People's Republic of China*

† Electronic Supplementary Information (ESI) available: [Additional device cross-section, GO morpholgies on ITO, transmittance of different substrates, morphologies and absorbances of perovskite films on different substrates and electrical characterization of devices with different hole conductors]. See DOI: 10.1039/b000000x/

1. S. B. Darling, F. You, T. Veselka and A. Velosa, *Energy Environ. Sci*, 2011, **4**, 3133.
2. J. You, C.-C. Chen, Z. Hong, K. Yoshimura, K. Ohya, R. Xu, S. Ye, J. Gao, G. Li and Y. Yang, *Adv. Mater.*, 2013, **25**, 3973.
3. J. You, L. Dou, K. Yoshimura, T. Kato, K. Ohya, T. Moriarty, K. Emery, C.-C. Chen, J. Gao and G. Li, *Nat. Commun.*, 2013, DOI: 10.1038/ncomms2411.
4. A. Yella, H.-W. Lee, H. N. Tsao, C. Yi, A. K. Chandiran, M. K. Nazeeruddin, E. W.-G. Diau, C.-Y. Yeh, S. M. Zakeeruddin and M. Grätzel, *Science*, 2011, **334**, 629.
5. I. Chung, B. Lee, J. He, R. P. Chang and M. G. Kanatzidis, *Nature*, 2012, **485**, 486.
6. J. Burschka, N. Pellet, S.-J. Moon, R. Humphry-Baker, P. Gao, M. K. Nazeeruddin and M. Grätzel, *Nature*, 2013, **499**, 316.
7. M. Liu, M. B. Johnston and H. J. Snaith, *Nature*, 2013, **501**, 395.
8. N.-G. Park, *J. Phys. Chem. Lett.*, 2013, **4**, 2423.
9. H. J. Snaith, *J. Phys. Chem. Lett.*, 2013, **4**, 3623.
10. A. Kojima, K. Teshima, Y. Shirai and T. Miyasaka, *J. Am. Chem. Soc.*, 2009, **131**, 6050.
11. M. M. Lee, J. Teuscher, T. Miyasaka, T. N. Murakami and H. J. Snaith, *Science*, 2012, **338**, 643.
12. B. Cai, Y. Xing, Z. Yang, W.-H. Zhang and J. Qiu, *Energy Environ. Sci.*, 2013, **6**, 1480.
13. H.-S. Kim, C.-R. Lee, J.-H. Im, K.-B. Lee, T. Moehl, A. Marchioro, S.-J. Moon, R. Humphry-Baker, J.-H. Yum and J. E. Moser, *Sci. Rep.*, 2012, DOI: 10.1038/srep00591.
14. J. H. Heo, S. H. Im, J. H. Noh, T. N. Mandal, C.-S. Lim, J. A. Chang, Y. H. Lee, H.-j. Kim, A. Sarkar and M. K. Nazeeruddin, *Nat. Photon*, 2013, **7**, 486.
15. J. M. Ball, M. M. Lee, A. Hey and H. J. Snaith, *Energy Environ. Sci.*, 2013, **6**, 1739.
16. J. H. Noh, S. H. Im, J. H. Heo, T. N. Mandal and S. I. Seok, *Nano Lett.*, 2013, **13**, 1764.
17. O. Malinkiewicz, A. Yella, Y. H. Lee, G. M. Espallargas, M. Graetzel, M. K. Nazeeruddin and H. J. Bolink, *Nat. Photon*, 2014, **8**, 128.
18. D. Liu and T. L. Kelly, *Nat. Photon*, 2013, **8**, 133.
19. S. D. Stranks, G. E. Eperon, G. Grancini, C. Menelaou, M. J. Alcocer, T. Leijtens, L. M. Herz, A. Petrozza and H. J. Snaith, *Science*, 2013, **342**, 341.
20. G. Xing, N. Mathews, S. Sun, S. S. Lim, Y. M. Lam, M. Grätzel, S. Mhaisalkar and T. C. Sum, *Science*, 2013, **342**, 344.
21. G. E. Eperon, V. M. Burlakov, P. Docampo, A. Goriely and H. J. Snaith, *Adv. Funct. Mater.*, 2014, **24**, 151.
22. B. Conings, L. Baeten, C. De Dobbelaere, J. D'Haen, J. Manca and H. G. Boyen, *Adv. Mater.*, 2013, **26**, 2041.
23. L. Etgar, P. Gao, Z. Xue, Q. Peng, A. K. Chandiran, B. Liu, M. K. Nazeeruddin and M. Grätzel, *J. Am. Chem. Soc.*, 2012, **134**, 17396.
24. A. Yella, L. P. Heiniger, P. Gao, M. K. Nazeeruddin and M. Gratzel, *Nano Lett*, 2014,14, 2591.
25. J. Y. Jeng, Y. F. Chiang, M. H. Lee, S. R. Peng, T. F. Guo, P. Chen and T. C. Wen, *Adv. Mater.*, 2013, **25**, 3727.
26. S. Sun, T. Salim, N. Mathews, M. Duchamp, C. Boothroyd, G. Xing, T. C. Sum and Y. M. Lam, *Energy Environ. Sci.*, 2014, **7**, 399.
27. C. Roldán-Carmona, O. Malinkiewicz, A. Soriano, G. M. Espallargas, A. Garcia, P. Reinecke, T. Kroyer, M. I. Dar, M. K. Nazeeruddin and H. J. Bolink, *Energy Environ. Sci.*, 2014, **7**, 994.
28. J. You, Z. Hong, Y. Yang, Q. Chen, M. Cai, T.-B. Song, C.-C. Chen, S. Lu, Y. Liu and H. Zhou, *ACS Nano*, 2014, **8**, 1674.
29. P. W. Liang, C. Y. Liao, C. C. Chueh, F. Zuo, S. T. Williams, X. K. Xin, J. Lin and A. K. Jen, *Adv Mater*, 2014,26, 3748.

30. J. Y. Jeng, K. C. Chen, T. Y. Chiang, P. Y. Lin, T. D. Tsai, Y. C. Chang, T. F. Guo, P. Chen, T. C. Wen and Y. J. Hsu, *Adv. Mater.*, 2014,26, 4107.
31. J. T.-W. Wang, J. M. Ball, E. M. Barea, A. Abate, J. A. Alexander-Webber, J. Huang, M. Saliba, I. Mora-Sero, J. Bisquert and H. J. Snaith, *Nano Lett.*, 2013, **14**, 724.
32. Z. Zhu, J. Ma, Z. Wang, C. Mu, Z. Fan, L. Du, Y. Bai, L. Fan, H. Yan and D. L. Phillips, *J. Am. Chem. Soc.*, 2014, **136**, 3760.
33. D. A. Schwartz, N. S. Norberg, Q. P. Nguyen, J. M. Parker and D. R. Gamelin, *J. Am. Chem. Soc.*, 2003, **125**, 13205.
34. Z. Liu, J. T. Robinson, X. Sun and H. Dai, *J. Am. Chem. Soc.*, 2008, **130**, 10876.
35. X. Sun, Z. Liu, K. Welsher, J. T. Robinson, A. Goodwin, S. Zaric and H. Dai, *Nano Research*, 2008, **1**, 203.
36. S.-S. Li, K.-H. Tu, C.-C. Lin, C.-W. Chen and M. Chhowalla, *ACS Nano*, 2010, **4**, 3169.
37. J. Liu, Y. Xue and L. Dai, *J. Phys. Chem. Lett.*, 2012, **3**, 1928.
38. Y. Gao, H. L. Yip, K. S. Chen, K. M. O'Malley, O. Acton, Y. Sun, G. Ting, H. Chen and A. K. Y. Jen, *Adv. Mater.*, 2011, **23**, 1903.
39. P. Docampo, J. M. Ball, M. Darwich, G. E. Eperon and H. J. Snaith, *Nat. Commun.*, 2013, DOI: 10.1038/ncomms3761.
40. C. S. Ponseca, T. J. Savenije, M. A. Abdellah, K. Zheng, A. P. Yartsev, T. Pascher, T. Harlang, P. Chabera, T. Pullerits and A. Stepanov, *J. Am. Chem. Soc.*, 2014, **136**, 5189.
41. H. J. Snaith, A. Abate, J. M. Ball, G. E. Eperon, T. Leijtens, N. K. Noel, S. D. Stranks, J. T.-W. Wang, K. Wojciechowski and W. Zhang, *J. Phys. Chem. Lett.*, 2014, **5**, 1511.
42. M. Saliba, K. W. Tan, H. Sai, D. T. Moore, T. Scott, W. Zhang, L. A. Estroff, U. Wiesner and H. J. Snaith, *J. Phys. Chem. C*, 2014, DOI: 10.1021/jp500717w.
43. K. W. Tan, D. T. Moore, M. Saliba, H. Sai, L. A. Estroff, T. Hanrath, H. J. Snaith and U. Wiesner, *ACS Nano*, 2014,8, 4730.

The Table of Contents

A champion efficiency of 12.4% is achieved for inverted planar heterojunction perovskite solar cell by employing graphene oxide as hole conductor.